Journal of Catalysis 442 (2025) 115911

Contents lists available at ScienceDirect

Journal of Catalysis

journal homepage: www.elsevier.com/locate/jcat

Research article

Molecularly modified aluminum phosphates as support materials for Ru nanoparticles in selective hydrogenation

Wenting Fang [a,b], Yuyan Zhang [b], Liqun Kang [a], Serena DeBeer [a], Walter Leitner [a], Alexis Bordet [a,*], Anders Riisager [b,*]

[a] Max Planck Institute for Chemical Energy Conversion, Stiftstraße 34–36, 45470 Mülheim an der Ruhr, Germany
[b] Centre for Catalysis and Sustainable Chemistry, Department of Chemistry, Technical University of Denmark, DK-2800 Kgs. Lyngby, Denmark

ARTICLE INFO

Keywords:
Aluminum phosphate
Surface molecular modification
Supported ionic liquid phase
Ru nanoparticles
Hydrogenation

ABSTRACT

Modified aluminum phosphate (APO-5) proved suitable as zeotype support for the preparation of imidazolium-based supported ionic liquid phase material, i.e. SILP(APO-5). The successful chemisorption of ionic liquid-like modifiers at the APO-5 surface was demonstrated by solid- state ^{31}P and ^{13}C nuclear magnetic resonance (NMR) spectroscopy. The immobilization of Ru nanoparticles (NPs) on SILP(APO-5) was achieved following an organometallic approach, producing well-dispersed Ru NPs with a mean average size of 1.4 nm on the support. The resulting Ru@SILP(APO-5) material was thoroughly characterized using multiple techniques, e.g., solid-state NMR, transmission electron microscopy (TEM), infrared (IR) spectroscopy, X-ray absorption spectroscopy (XAS), and applied as a catalyst for the hydrogenation of biomass-derived furfural acetone with molecular hydrogen. The ionic liquid-like layer was found beneficial for the stabilization of the Ru NPs as well as of the APO-5 material. A temperature-controlled selectivity switch between olefinic, carbonyl or furan ring hydrogenation could be achieved with this new material with the APO-5 facilitating activation of the olefinic bond, while the carbonyl bond was remarkably deactivated. The demonstrated suitability of aluminum phosphate materials to produce molecularly modified surfaces offers a new control parameter for the systematic design and optimization of zeotype-based catalysts.

1. Introduction

Aluminum phosphates, APO-*n* (with *n* denoting a particular structure type), are crystalline, microporous zeotype materials that possess silicon-free zeolite-like frameworks [1,2]. Their structure comprise three-dimensional channels composed of tetrahedrons of Al^{3+} and P^{5+} linked by oxygen atoms, resulting in theoretically neutral frameworks [3,4]. APO-*n* materials have good shape selectivity [5], thermal and hydrothermal stability [6,7], and their structure and compositional flexibility have made them very attractive in the field of catalysis, both at laboratory and industrial scale [2,8]. Their use include, for example, catalytic upgrading of alkanes [9–11], the conversion of methanol to olefins and dimethyl ether [12–15], and the decomposition of chloro-fluorocarbons [16].

Several strategies have been developed to incorporate acidic/basic sites in APO-*n*, including metal substitution [4,12], metal loading [17], and Al/P ratio adjustment [18]. APO-*n* are also an important family of support materials for metal nanoparticles (NPs) [19–22]. For example, Yang and co-workers reported the immobilization of Ni NPs on APO-5, and used the resulting catalyst for the hydrogenation of *α*-pinene [19]. Here, the pore size (3.95 nm) of APO-5 proved beneficial to facilitate the mass transfer of the substrate to the active sites, thereby enhancing activity and selectivity toward the formation of *cis*-pinane [19]. Metal NPs immobilized on acidic APO-*n* can also work as bifunctional catalysts. For example, Gao *et al.* used Pd/SAPO-5 (SAPO: silicoaluminophosphate) material for the one-pot aldol condensation between furfural and methyl isobutyl ketone, followed by hydrogenation with molecular hydrogen [20]. Recently, Fang *et al.* showed that Pd NPs supported on acidic APO-5 (Al/P ratio = 1.5) are efficient for the reductive etherification of furfural to ethyl furfuryl ether using formic acid as a hydrogen source [21]. In this case, the reductive etherification of furfural proceeded *via* initial acetalization catalyzed by the acidic APO-5 and subsequent hydrogenolysis catalyzed by the Pd NPs [21]. Hence, APO-*n* are established as support materials with tunable composition, crystallinity, and

* Corresponding authors.
E-mail addresses: alexis.bordet@cec.mpg.de (A. Bordet), ar@kemi.dtu.dk (A. Riisager).

https://doi.org/10.1016/j.jcat.2024.115911
Received 1 July 2024; Received in revised form 2 December 2024; Accepted 17 December 2024
Available online 24 December 2024

pore size that can influence the catalytic properties of metal NP catalysts [23].

In addition to changes in the intrinsic properties of support materials, molecular surface modification has recently emerged as a very promising strategy to influence and control the synthesis and catalytic performance of supported metal NPs [24–26]. In particular, monometallic and bimetallic NPs immobilized on SiO_2-based molecularly modified surfaces (NPs@MMS) have been explored for reactions involving the activation and the transfer of molecular hydrogen, such as selective hydrogenation [27–32], hydrodeoxygenation [33–36], and decarboxylation [37] reactions with reversible chemical changes of the modifier enabling the generation of adaptive catalytic systems [38,39]. Differently from SiO_2, the molecular surface modification of APO-*n* support materials has been scarcely explored [40]. In this context, we set our goal to explore the surface functionalization of APO-*n* materials with molecular modifiers, and to investigate its impact on the catalytic performance of immobilized metal NPs.

In the reported work, the surface molecular modification of a hydroxy-functionalized APO-5 support with an imidazolium-based ionic liquid (IL) is investigated. The resulting novel supported ionic liquid phase material, SILP(APO-5), is used to prepare catalyst materials by immobilizing Ru NPs *via* an organometallic approach (Fig. 1a). The textural, morphological, and electronic properties of the Ru@SILP(APO-5) catalyst are characterized using a combination of techniques including N_2 physisorption, solid-state nuclear magnetic resonance (NMR), powder X-ray diffraction (XRD), electron microscopy, and Ru K-edge X-ray absorption spectroscopy (XAS) (Fig. 1b). The impact of the molecular surface modification on the catalytic performance of Ru@SILP(APO-5) is examined for the hydrogenation of biomass-derived furfural acetone **1** with H_2 (Fig. 1c). This substrate contains a conjugated olefinic bond, an aromatic furan ring, and a carbonyl (ketone) functionality, and can be hydrogenated to different products, all considered potential fuels and fuel additives as well as interesting chemical building blocks [41].

2. Experimental

2.1. Materials

Phosphoric acid (H_3PO_4, 85 % aqueous solution, ≥99.8 %), aluminum isopropoxide ($Al(O\text{-}i\text{-}Pr)_3$, ≥98 %), triethylamine (Et_3N, ≥99 %), etidronic acid (EA, 60 % aqueous solution), hydrochloric acid (HCl, 37 %), methanol (≥99.9 %), sodium iodide (NaI, ≥99.5 %), 3-chloropropylethoxysilane (95 %), 1-butylimidazole (98 %), tetradecane (≥99 %), silica gel, and lithium bis(trifluoromethane)sulfonimide ($LiNTf_2$, 99.95 %) were purchased from Sigma-Aldrich. Bis(2-methylallyl)(1,5-cyclooctadiene)ruthenium(II) [$Ru(2\text{-methylallyl})_2(cod)$] (97 %), chloroform-d ($CDCl_3$, 99.8 %), and furfural acetone (**1**, 98 %) were obtained from abcr GmbH. Aluminum phosphate ($AlPO_4$) was purchased from Thermo Fisher Scientific. Acetone (≥99.5 %), toluene (≥99.5 %), dichloromethane (DCM, ≥99.5 %), pentane (≥99 %), ethyl acetate (≥99.5 %), diethyl ether (≥99.5 %) and 1,4-dioxane (≥99.5 %) were purchased from Carl Roth GmbH & Co. KG. All solvents were dried before being used, while other chemicals were used as received.

2.2. Synthesis of modified APO-5

The synthesis of modified APO-5 was based on a modified literature method [42–44] using a gel composition of $1Al_2O_3{:}1P_2O_5(H_3PO_4/EA = 2/1){:}1.5Et_3N{:}45H_2O$. Firstly, a solution of H_3PO_4 (3.84 g, 0.033 mol) and EA (5.73 g, 0.017 mol) in distilled water (24 mL) was vigorously stirred. Then $Al(O\text{-}i\text{-}Pr)_3$ (10.21 g, 0.05 mol) was added slowly to the solution, whereafter the mixture was stirred vigorously (1000 rpm) for 2 h. Subsequently, Et_3N (5.21 mL) was added slowly to the mixture followed by stirring (1000 rpm) for another 1 h and the solution was then transferred to a 200 mL Teflon lined hydrothermal autoclave, which was tightly closed and kept at 180 °C under autogenous pressure and static state for 48 h. After the crystallization reaction, the autoclave was cooled to room temperature and the obtained product washed with distilled water (3 × 100 mL) and oven (60 °C overnight) dried. The crude powder (1 g) was further treated twice with 0.1 M HCl in

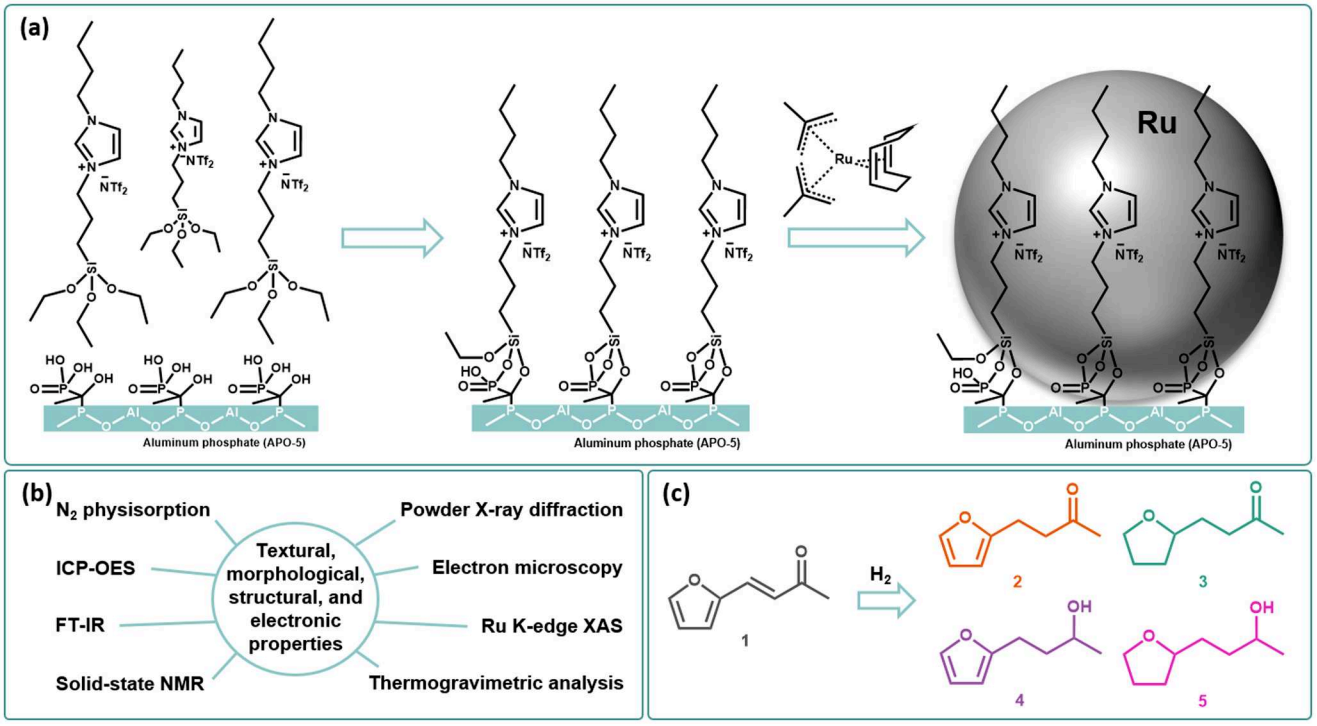

Fig. 1. (a) Synthesis pathway of the Ru@SILP(APO-5) catalyst; (b) Characterization methods used to investigate the prepared materials; (c) Possible products from the hydrogenation of furfural acetone **1** using Ru@SILP(APO-5) as catalyst.

methanol (2 × 100 mL) at 120 °C for 12 h in the autoclave to remove Et_3N and the obtained APO-5 finally washed with methanol (3 x 100 mL) and oven (60 °C overnight) dried.

2.3. Synthesis of SILP(support)

The IL 1-butyl-3-(3-triethoxysilylpropyl)imidazolium bis(trifluoromethylsulfonyl)imide (2.18 g, 3.55 mmol) prepared following a previously reported procedure (see SI for detailed procedure) [33,35], was added to a Schlenk flask in the glovebox and stirred (600 rpm) with 1,4-dioxane (2 mL) at room temperature until complete dissolution. APO-5 (1.0 g, dried *in vacuo* at 100 °C for 5 h), SiO_2 (1.0 g, dehydroxylated at 500 °C for 16 h) or $AlPO_4$ (1.0 g, dried *in vacuo* at 150 °C for 5 h) were added into another Schlenk flask and mixed with 1,4-dioxane (20 mL). The IL solution was then added to the suspension of the support material and stirred (600 rpm) under reflux (125 °C). After 18 h of reaction the mixture was cooled to room temperature, and the SILP material separated by filtration and washed with DCM (3 × 10 mL) followed by drying in *vacuo* ($1{\cdot}10^{-3}$ mbar, 60 °C). The 1,4-dioxane and DCM were collected to determine the amount of unreacted IL (96.1 wt %).

2.4. Synthesis of Ru@support

The procedure for the immobilization of Ru NPs on supports (SILP (APO-5), SILP(SiO_2), SILP($AlPO_4$), $AlPO_4$, or APO-5) was adapted from literature using a wet impregnation method [31,33]. The precursor [Ru(2-methylallyl)$_2$(cod)] (79.88 mg, 0.25 mmol) was dissolved in DCM (8 mL) and added to a suspension of support (500 mg) in DCM (12 mL). The reaction mixture was then stirred (800 rpm) at room temperature for 1 h, where after the DCM was removed under reduced pressure at room temperature and the impregnated support dried for another 1 h under the same conditions. The powder was then transferred into a 20 mL high-pressure autoclave and treated with H_2 (25 bar) at 100 °C for 18 h. After reduction, the color of the impregnated support transformed from white to light gray, indicating the formation of Ru NPs on the support.

2.5. Characterization and analysis

XRD data for phase analysis were obtained on a Rigaku SmartLab equipped with a rotating anode (9 kW, 45 kV, 200 mA) in Bragg-Brentano-geometry ($CuK_{\alpha1,2}$: 1.541862 Å). The data were collected with a HyPix-3000 multi-dimensional detector in 1D mode. The samples were placed on a quartz sample holder and data were collected continuously in the range of 5–50° 2θ in steps of 0.01° and a scan speed of 0.5° min^{-1}.

Brunauer-Emmett-Teller (BET) surface area and porosity analysis were conducted by N_2 physisorption performed at -196 °C by a Micromeritics ASAP 2020 instrument. Before the measurement the samples were degassed at 120 °C for 12 h.

Scanning electron microscopy (SEM) images were recorded on an AFEG 250 Analytical ESEM at 10 kV. Scanning transmission electron microscopy in high angle annular dark field (STEM-HAADF) was performed on a Hitachi HD-2700 cold FEG operated at 200 kV. Samples for electron microscopy were prepared by depositing the powder on a copper TEM grid with an amorphous carbon support film. To determine NPs size, at least 300–400 NPs were measured using ImageJ. Energy-dispersive X-ray (EDX) analysis was performed with an EDAX Octane T Ultra W 200 mm^2 SDD detector and TEAM software.

^1H and ^{13}C NMR spectra were obtained using a Bruker Avance 400TM spectrometer at 25 °C. ^{31}P and ^{29}Si magic-angle spinning (MAS) NMR spectra were performed on a Bruker AVANCE III HD spectrometer operating at a magnetic field of 14.05 T equipped with a 4 mm CP/MAS BBFO probe.

Inductively coupled plasma optical emission spectrometry (ICP-OES) was measured externally (Mikroanalytisches Laboratorium Kolbe, Oberhausen, Germany).

Thermogravimetric analysis (TGA) of samples was conducted under Helium flow from 40–800 °C on a Netzsch STA 409 with 10 °C min^{-1} heating rate.

Fourier-transform infrared spectroscopy (FT-IR) was performed on Shimadzu IRAffinity-1S from 4000–400 cm^{-1} at a resolution of 4 cm^{-1} averaging 40 scans for each measurement.

CO adsorbed FT-IR was performed by placing material (20 mg) into a Fisher-Porter bottle followed by vacuum treatment for 15 min (25 °C, $5.2{\cdot}10^{-2}$ mbar) and refilling the bottle with 3 bar CO gas. After 18 h, the CO gas was removed under vacuum (25 °C, $5.2{\cdot}10^{-2}$ mbar) and the sample pressed into a pellet using KBr (~30 mg), where after the IR spectrum was measured in a glovebox by a Thermo Scientific Nicolet™ iS5 spectrometer equipped with a transmission cell. The Ru K-edge (22117 eV) X-ray absorption fine structure (XAFS) spectra of the Ru samples were collected at the P65 beamline of PETRA III (P65 Applied X-ray Absorption Spectroscopy) [45]. At P65 beamline, monochromatic beam was introduced through an 11-period undulator and a Si (311) double crystal monochromator operated in QEXAFS mode with energy resolving power of ΔE/E of $6.0{\bullet}10^{-5}$. The beam size at the sample position was approx. 0.5 × 1.0 mm^2 (V × H), and the photon flux was ~10^{11} photons s^{-1} (without attenuation). For each sample, the powder of the sample was sealed by Kapton tape into an in-house designed PEEK-made powder cell. The amount of the powder was optimized based on the absorption cross-sections and the dimensions of the powder cells to obtain optimal transmission absorption (edge jump close to 1.0). The XAFS spectra for all samples were collected in transmission mode at -258 °C using a liquid He cryostat. The intensities of the incident beam (I_0) and the transmitted beam (I_t) were monitored by ionization chambers (filled with mixture of Kr and N_2). The energy range for the full XAFS spectra was 21917–23417 eV (k_{max} = 18.2) with energy step of 0.6 eV. The XAFS of each sample was measured three times and merged to improve the signal-noise ratio. Ru foil was measured simultaneously for each sample as the reference for energy calibration. The energy of the incident beam was calibrated by assigning the energy of the first inflection in the first derivative X-ray absorption near-edge structure (XANES) of Ru foil to 22,117 eV. In addition to Ru foil, commercial RuO_2 powder was also measured in transmission mode as references. The Ru K-edge XAS spectra were analyzed using the Demeter software package (including Athena and Artemis programs, version 0.9.26) [46]. Pre-edge background subtraction and post-edge normalization of the XAFS data were performed using the Athena program. A linear regression background in the range of 21917 to 22027 eV was determined, and a quadratic polynomial regression for post-edge normalization in the range of 22267 to 23387 eV was applied. The spectra were splined from k = 0 $Å^{-1}$ to k = 18 $Å^{-1}$ with rbkg of 1.0 and k-weight of 2. The fitting of extended X-ray absorption fine structure (EXAFS) spectra (R range: 1 to 3 Å, k range: 3.4 to 13.5 $Å^{-1}$) was performed using the Artemis program based on scattering paths generated from FEFF6. The amplitude reduction factor S_0^2 is determined to be 0.70 by fitting of k^2-weighted R-space EXAFS of Ru foil based on the standard crystal parameters of ruthenium metal (data from Crystal Open Database, entry ID: 9008513), and was used as fixed parameter for the EXAFS fitting of other Ru samples.

2.6. Catalytic reactions

In a typical experiment, **1** (54.5 mg, 0.40 mmol, 160 eq.), catalyst (5 mg, 2.5 μmol Ru, 1.0 eq.), and 1,4-dioxane (1 mL) were mixed in a glass inlet and placed in a 10 mL high-pressure autoclave. After purging the autoclave with H_2, the reaction mixture was pressurized under H_2 (30 bar), and magnetically stirred (500 rpm) at the desired temperature in an aluminum heating block. When the reaction was finished, the reactor was cooled down in a water bath and vented in a fume hood. The reaction solution was analyzed after filtration by gas chromatography with flame ionization detection (GC-FID) on a Shimadzu GC-2030

equipped with a CP-WAX-52CB column from Agilent using tetradecane as an internal standard. Gas chromatography coupled with a mass spectrometer (GC-MS) were performed on a Shimadzu QP2020. Error bars were obtained by three repeated reactions.

2.7. Catalyst recycling reactions

The reusability of Ru@SILP(APO-5) and Ru@APO-5 was examined for the hydrogenation of **1** at 120 °C in consecutive 16 h reactions. After each reaction, the catalyst was collected *via* centrifugation (2000 rpm, 10 min), washed with 1,4-dioxane (3 × 2 mL) and used directly for the next cycle.

3. Results and discussion

3.1. Synthesis and characterization of modified APO-5

The synthesis of modified APO-5 was achieved by alteration of a hydrothermal procedure reported previously [42–44] using a gel composition of $1Al_2O_3$:$1P_2O_5$:$1.5Et_3N$:$45H_2O$ with a 2/1 M ratio of H_3PO_4/etidronic acid (EA). EA was introduced as a new variant for APO-5 modification to generate the required surface hydroxyl functionalities needed for subsequent surface molecular modification, and the product was thoroughly washed with methanolic HCl solution to remove the Et_3N template.

The AFI-type structure of the synthesized APO-5 was confirmed by powder XRD characterization (Fig. S1) [47], and N_2 adsorption–desorption isotherms (Fig. S2) showed a BET surface area of 149 m^2 g^{-1} (Table S1) as well as the presence of both micropores and mesopores (pore size 29 nm). SEM revealed a spherical morphology of the APO-5 particles with a mean diameter of ca. 25 μm (Fig. S3). This size is noticeably different from APO-5 prepared using H_3PO_4 as the only P source (hexagon prism-like shape of ca. 5 μm) [48], and such morphological changes may originate from the differences in pH values of the gels when EA was used as a phosphorous co-source [49]. The ^{31}P MAS NMR spectrum of the synthesized APO-5 (Fig. 2a) showed a characteristic broad signal associated to $P(OAl)_4$ (δ -30 ppm) [50,51], with an additional broad signal (δ -23 ppm) corresponding to P-OH groups [52,53]. Furthermore, signals from EA (δ 19 and 71 ppm) [54], the P-source of APO-5, were observed in the ^{13}C MAS NMR spectrum (Fig. 2b) along with minor signals from Et_3N ($\delta \sim$ 5 and 45 ppm) [55] remaining after the HCl washing. Importantly, the shift of the XRD peaks (Fig. S1) and the P-OH signals in ^{31}P NMR (Fig. 2a) indicate the successful incorporation of EA into the APO-5 framework. In combination with the mesoporosity of the material originating from the framework distortion by the EA incorporation, this makes the EA-modified APO-5 a

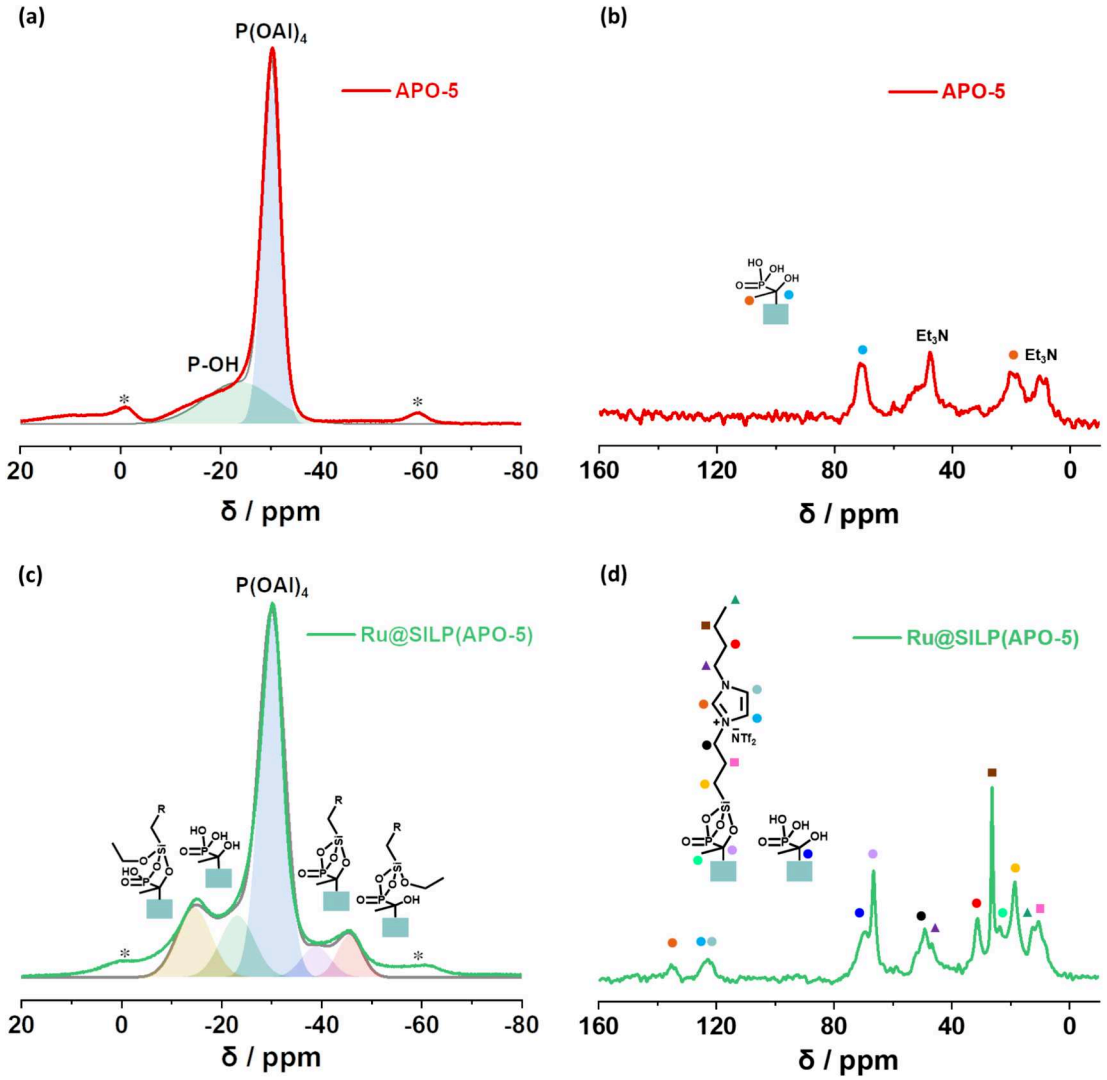

Fig. 2. (a) ^{31}P MAS NMR and (b) ^{13}C MAS NMR spectra of modified APO-5; (c) ^{31}P MAS NMR and (d) ^{13}C MAS NMR spectra of Ru@SILP(APO-5) (* corresponds to spinning bands).

potentially suitable support for the chemisorption of ILs.

3.2. Synthesis and characterization of Ru@SILP(APO-5)

Ru@SILP(APO-5) was prepared *via* a two-step procedure including the chemisorption of an imidazolium-based IL, and the immobilization of Ru NPs by an organometallic approach [56] (Fig. 1a). Reference materials Ru@APO-5, Ru@SILP(SiO_2), and Ru@SILP($AlPO_4$) were prepared following the same approach. First, the surface of the APO-5 material was molecularly modified through silanization with the well-known IL 1-butyl-3-(3-ethoxysilylpropyl)imidazolium bis(trifluoromethylsulfonyl)imide following a procedure previously reported for the silanization of ILs on SiO_2 [30]. The loading of IL-like modifier on APO-5 was estimated to be 0.14 mmol g^{-1} (Table S1) from the IL left in solution, corresponding to a surface coverage of 68 % (i.e., 6.39 mmol IL cm^{-2}) if assuming that all P-OH groups were exposed on the APO-5 surface. In the second step, Ru NPs were immobilized on the prepared SILP(APO-5) by wet impregnation using a solution of [Ru(2-methylallyl)$_2$(1,5-cyclooctadiene)] in DCM followed by heating under H_2 pressure (100 °C, 25 bar, 18 h), which resulted in the material changing from colorless to gray indicating the formation of Ru NPs on the support.

Characterization of the prepared Ru@SILP(APO-5) by ICP-OES showed a Ru loading of 4.5 wt%, which was coherent with the theoretical value expected from the impregnation (5 wt%). Moreover, ^{31}P MAS NMR analysis of the catalyst (Fig. 2c) showed signals (δ -30 ppm and -23 ppm) attributed to P(OAl)$_4$ and P-OH species [21,22], which were also observed for the APO-5 alone (Fig. 2a). In addition, three other signals (δ -45, -39, and -15 ppm) were detected and attributed to P-O-Si species [57,58] (Fig. 2c), providing evidence for the covalent attachment of the IL-like molecular structures on the APO-5 support. Consistent with this observation, ^{13}C MAS NMR evidenced also a signal (δ 66 ppm) characteristic of P-C-O-Si functionalities [59] (Fig. 2d). Signals attributed to the imidazolium ring and *N*-alkyl chain of the IL structure were also observed (Fig. 2d), indicating that the structure of the molecular modifier was not affected by the chemisorption step nor by the immobilization of Ru NPs. This is in line with the FT-IR spectrum of Ru@SILP(APO-5), which showed characteristic vibrations of C–H stretching bonds of the imidazolium ring and *N*-alkyl chain as well as symmetric ring stretches of the imidazolium moieties [31,60,61] (Fig. S4). TGA of Ru@SILP(APO-5) indicated a loading of IL-like modifier of 7.6 wt% (obtained from the comparison of APO-5 and SILP(APO-5)), in agreement with the 0.14 mmol g^{-1} estimated during synthesis, and a thermal stability up to ca. 260 °C (Figs. S5 and S6).

HAADF-STEM showed small and homogeneously dispersed Ru NPs for Ru@SILP(APO-5) as well as for Ru@APO-5, with NPs sizes of 1.4 and 1.1 nm, respectively (Fig. 3a-b). Such small size difference may be rationalized by the difference of the surface properties of the support materials with the IL-like layer providing an hydrophobic environment

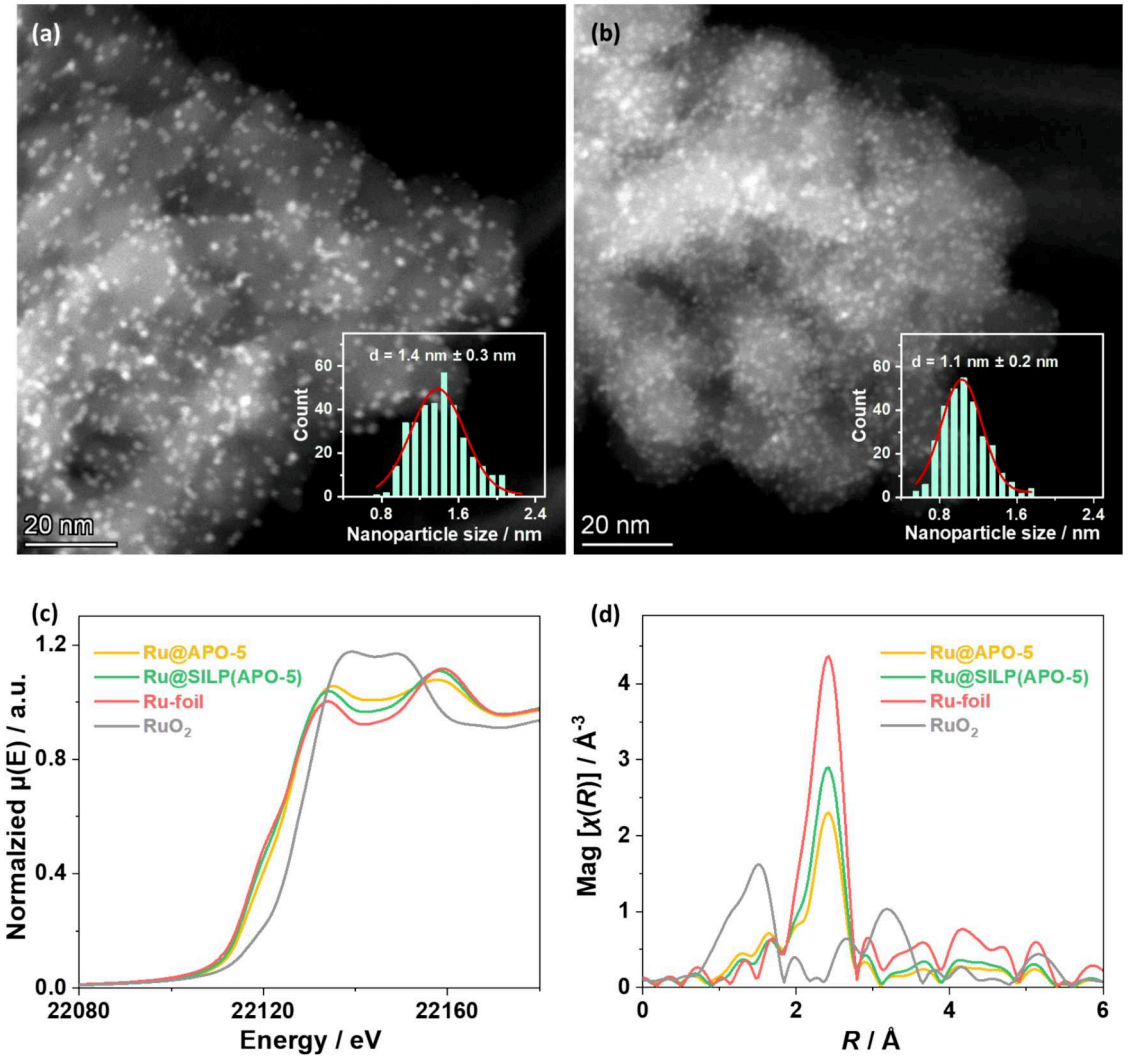

Fig. 3. HAADF-STEM of (a) Ru@SILP(APO-5) and (b) Ru@APO-5; (c) Ru K-edge normalized XANES spectra and (d) k^2-weighted R-space EXAFS spectra for Ru@APO-5, Ru@SILP(APO-5), Ru foil, and RuO_2 reference.

favoring Ru NPs growth on SILP(APO-5) [62], while the exposed P-OH groups on APO-5 can potentially inhibit NPs growth [63]. STEM-HAADF-EDX images also corroborated that the Ru NPs and the IL-like layer were homogeneously distributed on the APO-5 materials (Fig. S7). In addition, FT-IR measurements on Ru@APO-5 and Ru@SILP (APO-5) using CO as a molecular probe evidenced linear and bridged CO species on both materials (Fig. S8) [64,65], but also a significant red shift of these bands for Ru@SILP(APO-5), from 2076 to 2065 cm^{-1} and from 2017 to 1991 cm^{-1}, for linear and bridged CO species, respectively. This red shift of CO bands in the presence of the IL-like layer indicates that the electronic field of the Ru NPs [66,67], is increased due to an interaction between the NPs and the IL layer.

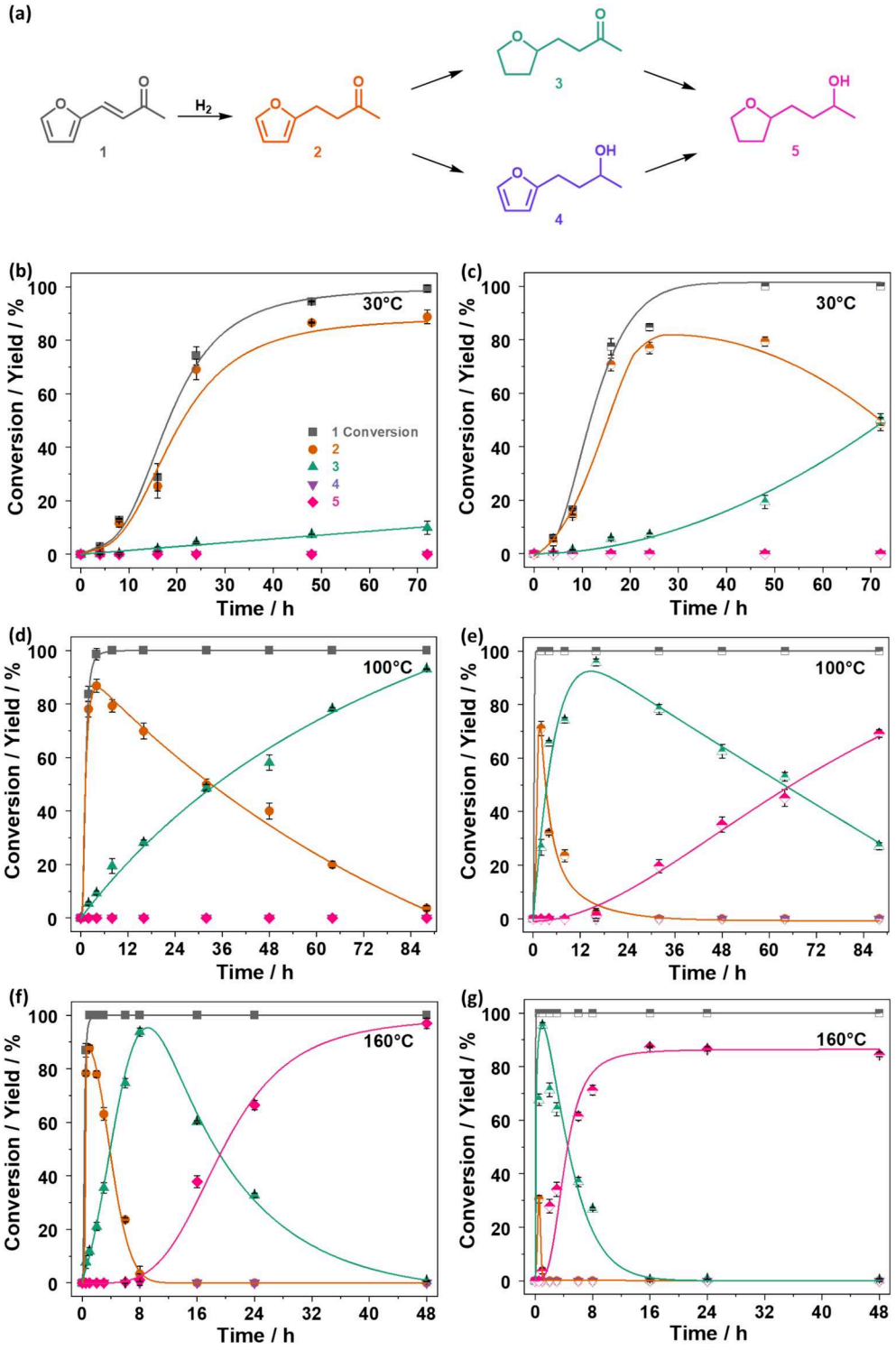

Fig. 4. (a) Pathway of furfural acetone **1** hydrogenation and reaction profiles for the hydrogenation using Ru@SILP(APO-5) (left) and Ru@APO-5 (right) at different reaction temperatures (b-c) 30 °C, (d-e) 100 °C, and (f-g) 160 °C. Reaction conditions: **1** (54.5 mg, 0.4 mmol, 160 eq.), catalyst (5 mg, 0.0025 mmol Ru), 1,4-dioxane (1 mL), H_2 (30 bar). Symbol codes: grey square – conversion; orange circle – yield of **2**; green triangle – yield of **3**; and pink diamond – yield of **5**. Data points are the average values of three experiments, and error bars represent standard deviations. (For interpretation of the references to color in this figure legend, the reader is referred to the web version of this article.)

To comprehensively analyze the electronic and geometric structure of the Ru@SILP(APO-5) and Ru@APO-5 catalysts, Ru K-edge XANES and EXAFS measurements were performed as illustrated in Fig. 3c-d. The absorption edge position of Ru@SILP(APO-5) aligns closely with that of the Ru foil, suggesting that the Ru species in the catalyst predominantly exist in a zerovalent state. In contrast, the XANES of Ru@APO-5 displays a slight shift towards higher energy level compared to Ru@SILP(APO-5), indicating a higher degree of Ru oxidation for Ru@APO-5. This agrees well with EXAFS fitting results (Figs. S9 and S10, Table S2), showing a coordination number (C.N.) of 1.0 ± 0.4 for Ru-O in Ru@SILP(APO-5), which is significantly lower than in Ru@APO-5 (C.N. = 2.1 ± 0.3).

Considering that both catalysts were stored and handled in air, the presence of oxidized Ru species on the surface of the Ru NPs was inevitable in both materials. The higher degree of oxidation in Ru@APO-5 most likely originated from its slightly smaller Ru NPs, in which the proportion of surface oxidation is larger. However, the IL may also provide some protection from oxidation to Ru NPs in Ru@SILP(APO-5) [68].

3.3. Catalytic study

The catalytic properties of Ru@SILP(APO-5) and Ru@APO-5 as a reference catalyst were investigated for the hydrogenation of the furanic α,β-unsaturated ketone furfural acetone **1** (**1**/Ru molar ratio of 160/1). The initial hydrogenation of **1** (Fig. 4a) is expected to occur with the olefinic C=C bond to form 4-(2-furyl)butan-2-one **2**. Next, hydrogenation of the furan ring forms 4-(tetrahydro-2-furyl)butan-2-one **3** followed by reduction of the carbonyl group to produce 4-(tetrahydro-2-furyl)butan-2-ol **5**. The alternative sequence where the hydrogenation of the ketone in **2** produces 4-(2-furyl)butan-2-ol **4** prior to the reduction of the furan ring, is less preferred over Ru catalysts [39].

Time profiles for the hydrogenations of **1** with Ru@SILP(APO-5) or Ru@APO-5 as catalysts, 1,4-dioxane as a solvent, and pressurized with H_2 (30 bar) were recorded at three different temperatures (30, 100, and 160 °C) using magnetically stirred high-pressure batch reactors (Fig. 4b-g). At 30 °C, Ru@SILP(APO-5) was active mainly for the hydrogenation of the conjugated C=C bond giving **2** in high yield and selectivity (89 %) after 72 h with marginal furan ring hydrogenation and only traces of **3** (Fig. 4b). The induction period observed at short reaction times is presumably related to the slow reduction of the slight amount of surface Ru oxide species (suggested by XANES and EXAFS) at this temperature. At 100 °C, **1** was rapidly hydrogenated to **2** (87 % yield after 4 h), followed by furan ring hydrogenation to give **3** selectively in high yield (93 %) after 88 h (Fig. 4d). C=O hydrogenation activity was unlocked at 160 °C, giving a time profile typical of sequential hydrogenation reactions (Fig. 4f). This allowed achieving highly selective C=C hydrogenation (87 % yield of **2** after 1 h) followed by furan ring hydrogenation (94 % yield of **3** after 8 h), and finally complete hydrogenation to product **5** (97 % yield) after 48 h. The observed hydrogenation pathway *via* the saturated ketone **3** instead of the unsaturated alcohol **4** is typical for Ru and Rh NPs-based catalysts, as previously described [30,39].

Determination of activation energies (Fig. S11) for the hydrogenation steps gave $E_{a(C=C)}$ (53.5 kJ mol^{-1}) ≪ $E_{a(Furan\ ring)}$ (84.5 kJ mol^{-1}) < $E_{a(C=O)}$ (98.8 kJ mol^{-1}). These relatively high energy barriers between the different hydrogenation steps corroborate with the hydrogenation proceeding essentially stepwise. Thus, the chemoselectivity of Ru@SILP (APO-5) can be easily tuned toward three different hydrogenation products of **1** in high yield without formation of byproducts by simple adjustment of the reaction temperature or time. In contrast, Ru@APO-5 showed a higher total activity (Fig. 4c,e,g), which may be at least partially linked to its smaller Ru NPs size and no influence of IL. However, Ru@APO-5 typically yielded product mixtures and failed overall to reach the level of selectivities of Ru@SILP(APO-5) under the applied reaction conditions, especially for products **2** (maximum yield of 79 % at 30 °C) and **5** (maximum yield of 87 % at 160 °C). The energy barriers between the hydrogenation steps ($E_{a(C=C)}$ = 37.2 kJ mol^{-1} ~ $E_{a(Furan\ ring)}$ = 41.7 kJ mol^{-1} < $E_{a(C=O)}$ = 64.0 kJ mol^{-1}, Fig. S11) were found lower than for Ru@SILP(APO-5), consistent with the difficulty to target selectively the different hydrogenation products by tuning the reaction conditions. Side product formation was not completely avoided at 160 °C (e.g., degradation and hydrodeoxygenation; Fig. S12), presumably due to exposure to P-OH functionalities on the catalyst surface.

Thus, the presence of the IL surface modification appears crucial to prevent side-reactions catalyzed by exposed P-OH functionalities, as well as to tune the electronic properties of Ru NPs and facilitate the kinetic control of product selectivity. In addition, a potential influence of the IL-like layer on the local concentration of substrate and/or H_2 cannot be ruled out.

Replacing the APO-5 support with SiO_2 support produced the previously reported Ru@SILP(SiO_2) catalyst [56]. Ru@SILP(SiO_2) was found more active, with rapid hydrogenation to the fully saturated product **5** also at moderate temperatures, and the selectivity towards product **2** remained poor even when lowering the H_2 pressure to 10 bar (Table S3). While some of this activity improvement may come from the higher surface area of the SiO_2 support, the interaction of **1** with SILP (APO-5), Ru@SILP(APO-5), SILP(SiO_2), and Ru@SILP(SiO_2) was probed by FT-IR (Fig. 5 and Fig. S13). Interestingly, a significant blue shift (from 1655 to 1664 cm^{-1}) of the band characteristic of the C=O in **1** was observed on SILP(APO-5) and Ru@SILP(APO-5), but not on SILP (SiO_2) and Ru@SILP(SiO_2). This blue shift indicates a shortening of the C=O bond in **1**, and thus a deactivation of the ketone for hydrogenation [69,70]. These findings are consistent with the slower hydrogenation of **3** to **5** observed with the APO-5-based catalysts, and evidence their specificity as compared to other supports such as SiO_2. In contrast, a red shift was observed for the band characteristic of the conjugated C=C bond, indicating an activation [71,72].

Commercial amorphous $AlPO_4$ was also tested for the preparation of Ru@SILP($AlPO_4$) and Ru@$AlPO_4$ materials. Interestingly, the SILP preparation was poorly successful, with an IL loading of only 0.039 $mmol_{IL}$ g^{-1} as determined by TGA (Fig. S14). Furthermore, STEM-HAADF and STEM-HAADF-EDX images (Figs. S15 and S16) showed large Ru NPs and severe aggregation on both Ru@SILP($AlPO_4$) and Ru@$AlPO_4$. The challenges in the SILP and Ru NPs preparation presumably originate from the very small BET surface area of the commercial $AlPO_4$ material (Table S1). While Ru@SILP($AlPO_4$) and Ru@$AlPO_4$ showed high activity toward product **5** (Table S3), they

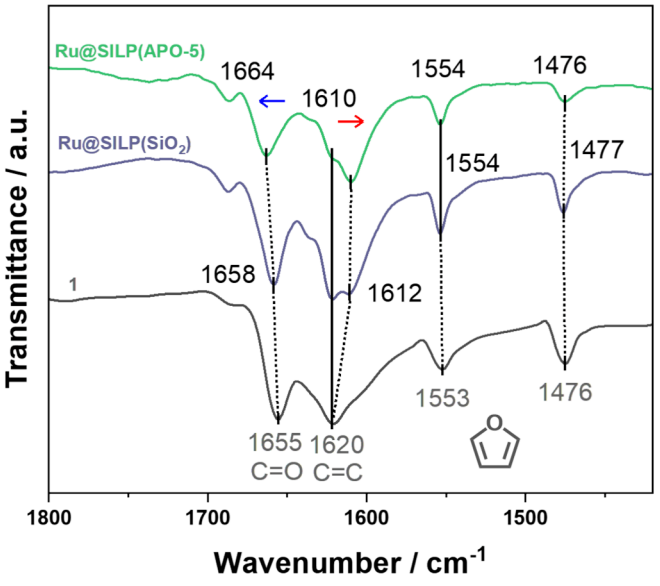

Fig. 5. FT-IR spectra of furfural acetone **1** and adsorbed **1** on Ru@SILP(APO-5) and Ru@SILP(SiO_2).

failed to provide high yields of the equally important intermediate compound **2** (Table S4).

The reusability and stability of the Ru@SILP(APO-5) and Ru@APO-5 catalysts were investigated for consecutive hydrogenation reactions of **1** under identical conditions (120 °C, 16 h, 30 bar H_2). The temperature of 120 °C was selected as a relatively high reaction temperature providing a distribution of different products. Ru@SILP(APO-5) proved reusable in at least eight consecutive hydrogenation reactions with unchanged product distribution (Fig. 6a), and HAADF-STEM analysis of the catalyst after the eight reaction runs (Fig. 6c) did not reveal any change in the size of the comprised Ru NPs (1.5 ± 0.2 nm *vs* 1.4 ± 0.3 nm for the fresh Ru NPs; Fig. 3a), evidencing their excellent stability. The enhanced stability of metal NPs in SILP environment is consistent with previous reports, and attributed to the electrosteric stabilization of NPs by the IL-like layer in addition to the stabilization from the support material [30,73–75]. Also, ICP-OES analysis and N_2 adsorption experiments (Table S1) did not evidence noticeable changes in Ru loading nor in the BET surface area, indicating that the catalyst did not suffer from leaching of Ru metal and IL-like molecular modifier. The presence of the IL-like layer on the catalyst after reaction was further confirmed by TGA and FT-IR analyses (Figs. S17 and S18). Moreover, the APO-5 retained its AFI structure with only a very slight change in the XRD diffractogram with the formation of some new phases (Fig. S19). When reusing Ru@APO-5 for the hydrogenation of **1**, the product distribution changed significantly in consecutive catalytic runs with an apparent increase in activity until the fifth reaction run followed by a progressive deactivation (Fig. 6b). Determination of the Ru NPs mean size in the catalyst by HAADF-STEM revealed that initially small and narrow-sized Ru NPs (1.1 ± 0.2 nm; Fig. 3b) aggregated into irregularly shaped and larger Ru NPs (2.1 ± 0.7 nm) with wider size distribution (Fig. 6d). Thus, the fluctuation in activity is presumably linked to the evolution of the NP size through a typical NP size effect, consistent with previous observations of Rh NPs of similar sizes used in the hydrogenation of the same substrate [30]. In addition, ICP-OES analysis showed a decreased Ru loading after reuse for the reaction runs (from 4.92 to 2.62 wt%), indicating a severe leaching of Ru during catalysis. The BET surface area also decreased substantially (from 66.8 to 38.7 $m^2\ g^{-1}$), probably due to the accumulation of substrate/products on the catalyst surface as evidenced by FT-IR [76] (Fig. S20) and the formation of new phases of APO-5 as observed by powder XRD (Fig. S21). A relatively large mass loss measured by TGA for the catalyst above 520 °C can likely also be associated to new phases formed under reaction conditions (Fig. S22). Hence, IL chemisorption could stabilize both the Ru NPs and the APO-5 support under operating conditions.

4. Conclusions

The surface molecular modification of APO-5 comprising surface hydroxyl groups, mesosporosity, and intercrystallinity was demonstrated with an imidazolium-based IL-like layer. Characterization of the novel SILP(APO-5) material confirmed the IL to be successfully grafted on the support, and when the material was used to immobilize Ru NPs following an organometallic approach the resulting Ru@SILP(APO-5) catalyst contained well-dispersed metallic Ru NPs with an average size of 1.4 nm. The Ru@SILP(APO-5) catalyst exhibited a high, yet somewhat tamed catalytic activity for hydrogenation as compared to a reference material Ru@APO-5 without the IL-like modifier. Nevertheless, the modified catalyst exhibited excellent product selectivity control in the stepwise hydrogenation of furfural acetone **1** (30 bar H_2) by the adjustment of reaction temperature (or reaction time), due to activation of the C═C bond and deactivation of the C═O bond upon catalyst adsorption as well as energy barriers between the different hydrogenation steps. This allowed providing high selectivity for olefinic reduction (**2**, 83 % yield, 30 °C), olefinic/furan ring reduction (**3**, 99 % yield,

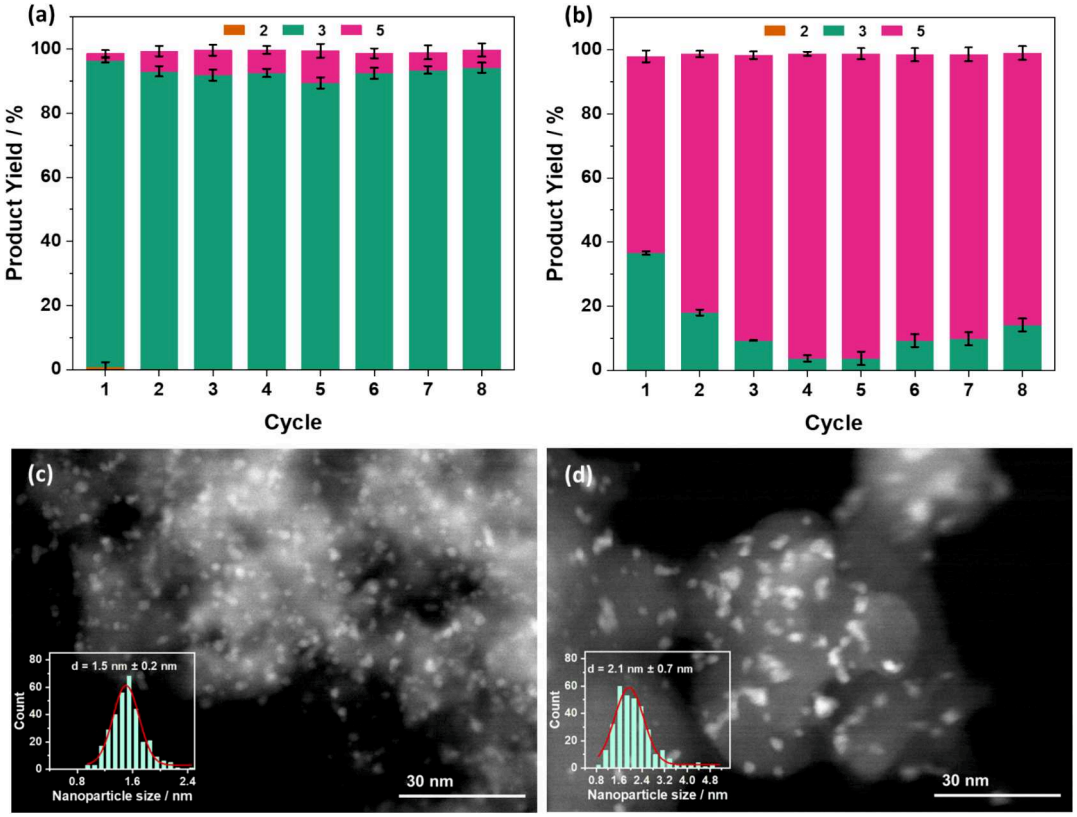

Fig. 6. Reusability of (a) Ru@SILP(APO-5) and (b) Ru@APO-5 in the hydrogenation of furfural acetone **1**. Reaction conditions: **1** (109 mg, 0.8 mmol, 40 eq.), catalyst (40 mg, 0.02 mmol Ru), 1,4-dioxane (2 mL), H_2 (30 bar), 120 °C, 16 h. The conversion was 100 % in all reactions. Data points are average values of three experiments, and error bars represent standard deviations. STEM-HAADF of (c) Ru@SILP(APO-5) and (d) Ru@APO-5 after eight reaction runs, respectively.

100 °C) or olefinic/furan ring/carbonyl group reduction (**5**, 97 % yield 160 °C), respectively. Importantly, the chemisorbed IL stabilized both the immobilized Ru NPs and the APO-5 support during the catalytic reactions leading to high stability and reusability of the Ru@SILP(APO-5) catalyst with constant performance over eight consecutive reaction runs, which was not the case for the reference catalyst Ru@APO-5. These results demonstrate that the concept of surface molecular modification is compatible with the use of aluminum phosphate materials, offering a new control parameter for the systematic design and optimization of zeotype-based MMS catalysts.

CRediT authorship contribution statement

Wenting Fang: Writing – original draft, Methodology, Investigation. **Yuyan Zhang:** Writing – original draft, Methodology, Investigation. **Liqun Kang:** Writing – review & editing, Resources. **Serena DeBeer:** Writing – review & editing, Resources. **Walter Leitner:** Writing – review & editing, Supervision, Resources. **Alexis Bordet:** Writing – review & editing, Supervision, Methodology, Conceptualization. **Anders Riisager:** Writing – review & editing, Supervision, Methodology, Conceptualization.

Declaration of competing interest

The authors declare that they have no known competing financial interests or personal relationships that could have appeared to influence the work reported in this paper.

Acknowledgements

W.F. acknowledges the China Scholarship Council, China (No. 201908330324) and Otto Mønsteds Fond for awarding scholarships. The Department of Chemistry, Technical University of Denmark, the Max Planck Society and the Deutsche Forschungsgemeinschaft, under Germany's Excellence Strategy – Exzellenzcluster 2186 'The Fuel Science Center' (No. 390919832) are acknowledged for supporting the work. Claudia Weidenthaler is acknowledged for XRD measurements, Norbert Pfänder is thanked for performing electron microscopy, and Annika Gurowski, Alina Jakubowski and Justus Werkmeister for GC, GC-MS, and FT-IR measurements. PETRA III (Germany) is also acknowledged for the experiment time at P65 Applied XAFS beamline (proposal No. I-20220137), and Dr. Edmund Welter is thanked for assistance and support in using the beamline. L.K. acknowledges the Alexander von Humboldt Foundation for a postdoctoral fellowship and funding support.

Appendix A. Supplementary data

Supplementary data to this article can be found online at https://doi.org/10.1016/j.jcat.2024.115911.

Data availability

Data will be made available on request.

References

[1] S.T. Wilson, B.M. Lok, C.A. Messina, T.R. Cannan, E.M. Flanigen, Aluminophosphate molecular sieves: a new class of microporous crystalline inorganic solids, J. Am. Chem. Soc. 104 (1982) 1146–1147.
[2] J. Yu, R. Xu, Insight into the construction of open-framework aluminophosphates, Chem. Soc. Rev. 35 (2006) 593–604.
[3] B.M. Weckhuysen, R.R. Rao, J.A. Martens, R.A. Schoonheydt, Transition metal ions in microporous crystalline aluminophosphates: isomorphous substitution, Eur. J. Inorg. Chem. 565–577 (1999).
[4] S. Prasad, I. Balakrishnan, Bifunctional catalytic centres in cobalt substituted aluminophosphate molecular sieve, CoAPO-11, Catal. Lett. 11 (1991) 105–110.
[5] W. Fang, S. Liu, L. Schill, M. Kubus, T. Bligaard, A. Riisager, On the role of Zr to facilitate the synthesis of diesel and jet fuel range intermediates from biomass-derived carbonyl compounds over aluminum phosphate, Appl. Catal. B: Environ. 320 (2023) 121936.
[6] P. Del Campo, C. Martinez, A. Corma, Activation and conversion of alkanes in the confined space of zeolite-type materials, Chem. Soc. Rev. 50 (2021) 8511–8595.
[7] L. Yang, C. Wang, L. Zhang, W. Dai, Y. Chu, J. Xu, G. Wu, M. Gao, W. Liu, Z. Xu, P. Wang, N. Guan, M. Dyballa, M. Ye, F. Deng, W. Fan, L. Li, Stabilizing the framework of SAPO-34 zeolite toward long-term methanol-to-olefins conversion, Nat. Commun. 12 (2021) 4661.
[8] M.R. Agliullin, B.I. Kutepov, V.A. Ostroumova, A.L. Maximov, Silicoaluminophosphate Molecular Sieves SAPO-11 and SAPO-41: Synthesis, Properties, and Applications for Hydroisomerization of C_{16+} n-Paraffins. Part 1: Current State of Research on SAPO-11 and SAPO-41 Synthesis (A Review), Pet. Chem. 61 (2021) 836–851.
[9] E.T.C. Vogt, G.T. Whiting, A. Dutta Chowdhury, B.M. Weckhuysen, Chapter Two - Zeolites and Zeotypes for Oil and Gas Conversion, in: F.C. Jentoft (Ed.), Advances in Catalysis, Academic Press, 2015, pp. 143–314.
[10] J.M. Thomas, R. Raja, G. Sankar, R.G. Bell, Molecular sieve catalysts for the regioselective and shape-selective oxyfunctionalization of alkanes in air, Acc. Chem. Res. 34 (2001) 191–200.
[11] H. Oikawa, Y. Shibata, K. Inazu, Y. Iwase, K. Murai, S. Hyodo, G. Kobayashi, T. Baba, Highly selective conversion of ethene to propene over SAPO-34 as a solid acid catalyst, Appl. Catal. A: Gen. 312 (2006) 181–185.
[12] J. Xie, D.S. Firth, T. Cordero-Lanzac, A. Airi, C. Negri, S. Oien-Odegaard, K. P. Lillerud, S. Bordiga, U. Olsbye, MAPO-18 catalysts for the methanol to olefins process: influence of catalyst acidity in a high-pressure syngas (CO and H_2) environment, ACS Catal. 12 (2022) 1520–1531.
[13] U. Olsbye, S. Svelle, K.P. Lillerud, Z.H. Wei, Y.Y. Chen, J.F. Li, J.G. Wang, W.B. Fan, The formation and degradation of active species during methanol conversion over protonated zeotype catalysts, Chem. Soc. Rev. 44 (2015) 7155–7176.
[14] U. Olsbye, S. Svelle, M. Bjorgen, P. Beato, T.V. Janssens, F. Joensen, S. Bordiga, K. P. Lillerud, Conversion of methanol to hydrocarbons: how zeolite cavity and pore size controls product selectivity, Angew. Chem. Int. Ed. 51 (2012) 5810–5831.
[15] A. Airi, A. Damin, J. Xie, U. Olsbye, S. Bordiga, Catalyst sites and active species in the early stages of MTO conversion over cobalt AlPO-18 followed by IR spectroscopy, Catal. Sci. Technol. 12 (2022) 2775–2792.
[16] Y. Takita, H. Wakamatsu, G.-L. Li, Y. Moro-oka, H. Nishiguchi, T. Ishihara, Decomposition of chlorofluorocarbons over metal phosphate catalysis II. Origin of the stability of $AlPO_4$ and the location of Ce as a promoter, J. Mol. Catal. A Chem. 155 (2000) 111–119.
[17] M. Hartmann, L. Kevan, Transition-metal ions in aluminophosphate and silicoaluminophosphate molecular sieves: location, interaction with adsorbates and catalytic properties, Chem. Rev. 99 (1999) 635–663.
[18] W. Fang, A. Riisager, Improved catalytic transfer hydrogenation of biomass-derived aldehydes with metal-loaded aluminum phosphate, ACS Sustain. Chem. Eng. 10 (2022) 1536–1543.
[19] C. Yang, B. Xiang, L. Jiang, F. Zhang, C. Liu, Y. Wang, Y. Zheng, Z. Liu, P. He, Selective hydrogenation of α-pinene on a nickel supported aluminophosphate catalyst: process optimization and reaction kinetics, Int. J. Chem. Kinet. 53 (2020) 440–456.
[20] L. Gao, I. Miletto, C. Ivaldi, G. Paul, L. Marchese, S. Coluccia, F. Jiang, E. Gianotti, M. Pera-Titus, Rational design of bifunctional hierarchical Pd/SAPO-5 for the synthesis of tetrahydrofuran derivatives from furfural, J. Catal. 397 (2021) 75–89.
[21] W. Fang, J. Egebo, L. Schill, H. Chen, A. Riisager, Reductive etherification of furfural *via* hydrogenolysis with Pd-modified aluminum phosphate and formic acid, Green Chem. 24 (2022) 7346–7349.
[22] A. Kumar, R. Bal, R. Srivastava, Modulation of Ru and Cu nanoparticle contents over CuAlPO-5 for synergistic enhancement in the selective reduction and oxidation of biomass-derived furan based alcohols and carbonyls, Catal. Sci. Technol. 11 (2021) 4133–4148.
[23] T.W. van Deelen, C. Hernández Mejía, K.P. de Jong, Control of metal-support interactions in heterogeneous catalysts to enhance activity and selectivity, Nat. Catal. 2 (2019) 955–970.
[24] A. Bordet, W. Leitner, Metal nanoparticles immobilized on molecularly modified surfaces: versatile catalytic systems for controlled hydrogenation and hydrogenolysis, Acc. Chem. Res. 54 (2021) 2144–2157.
[25] T. Jiang, Y. Zhou, S. Liang, H. Liu, B. Han, Hydrogenolysis of glycerol catalyzed by Ru-Cu bimetallic catalysts supported on clay with the aid of ionic liquids, Green Chem. 11 (2009).
[26] R. Tao, S. Miao, Z. Liu, Y. Xie, B. Han, G. An, K. Ding, Pd nanoparticles immobilized on sepiolite by ionic liquids: efficient catalysts for hydrogenation of alkenes and heck reactions, Green Chem. 11 (2009) 96–101.
[27] S.J. Louis Anandaraj, L. Kang, S. DeBeer, A. Bordet, W. Leitner, Catalytic hydrogenation of CO_2 to formate using ruthenium nanoparticles immobilized on supported ionic liquid phases, Small 19 (2023) e2206806.
[28] S. Sisodiya-Amrute, C. Van Stappen, S. Rengshausen, C. Han, A. Sodreau, C. Weidenthaler, S. Tricard, S. DeBeer, B. Chaudret, A. Bordet, W. Leitner, Bimetallic M_xRu_{100-x} nanoparticles (M = Fe, Co) on supported ionic liquid phases (M_xRu_{100-x}@SILP) as hydrogenation catalysts: influence of M and M:Ru ratio on activity and selectivity, J. Catal. 407 (2022) 141–148.
[29] S. Rengshausen, C. Van Stappen, N. Levin, S. Tricard, K.L. Luska, S. DeBeer, B. Chaudret, A. Bordet, W. Leitner, Organometallic synthesis of bimetallic cobalt-rhodium nanoparticles in supported ionic liquid phases (Co_xRh_{100-x}@SILP) as catalysts for the selective hydrogenation of multifunctional aromatic substrates, Small 17 (2021) e2006683.

[30] A. Bordet, G. Moos, C. Welsh, P. Licence, K.L. Luska, W. Leitner, Molecular control of the catalytic properties of rhodium nanoparticles in supported ionic liquid phase (SILP) systems, ACS Catal. 10 (2020) 13904–13912.

[31] S. El Sayed, A. Bordet, C. Weidenthaler, W. Hetaba, K.L. Luska, W. Leitner, Selective hydrogenation of benzofurans using ruthenium nanoparticles in Lewis acid-modified ruthenium-supported ionic liquid phases, ACS Catal. 10 (2020) 2124–2130.

[32] S. Kacem, M. Emondts, A. Bordet, W. Leitner, Selective hydrogenation of fluorinated arenes using rhodium nanoparticles on molecularly modified silica, Catal. Sci. Technol. 10 (2020) 8120–8126.

[33] L. Goclik, H. Walschus, A. Bordet, W. Leitner, Selective hydrodeoxygenation of acetophenone derivatives using a $Fe_{25}Ru_{75}$@SILP catalyst: a practical approach to the synthesis of alkyl phenols and anilines, Green Chem. 24 (2022) 2937–2945.

[34] G. Moos, M. Emondts, A. Bordet, W. Leitner, Selective hydrogenation and hydrodeoxygenation of aromatic ketones to cyclohexane derivatives using a Rh@SILP catalyst, Angew. Chem. Int. Ed. 59 (2020) 11977–11983.

[35] L. Goclik, L. Offner-Marko, A. Bordet, W. Leitner, Selective hydrodeoxygenation of hydroxyacetophenones to ethyl-substituted phenol derivatives using a FeRu@SILP catalyst, Chem. Commun. 56 (2020) 9509–9512.

[36] L. Offner-Marko, A. Bordet, G. Moos, S. Tricard, S. Rengshausen, B. Chaudret, K. L. Luska, W. Leitner, Bimetallic nanoparticles in supported ionic liquid phases as multifunctional catalysts for the selective hydrodeoxygenation of aromatic substrates, Angew. Chem. 57 (2018) 12721–12726.

[37] S. Rengshausen, F. Etscheidt, J. Großkurth, K. Luska, A. Bordet, W. Leitner, Catalytic hydrogenolysis of substituted diaryl ethers by using ruthenium nanoparticles on an acidic supported ionic liquid phase (Ru@SILP-SO_3H), Synlett 30 (2019) 405–412.

[38] A. Bordet, W. Leitner, Adaptive catalytic systems for chemical energy conversion, Angew. Chem. Int. Ed. (2023) e202301956.

[39] A. Bordet, S. El Sayed, M. Sanger, K.J. Boniface, D. Kalsi, K.L. Luska, P.G. Jessop, W. Leitner, Selectivity control in hydrogenation through adaptive catalysis using ruthenium nanoparticles on a CO_2-responsive support, Nat. Chem. 13 (2021) 916–922.

[40] I.A. Auwal, K.-L. Wong, T.C. Ling, B.S. Ooi, E.-P. Ng, Metal chlorides grafted on SAPO-5 (MCl_x/SAPO-5) as reusable and superior catalysts for acylation of 2-methylfuran under non-microwave instant heating condition, Processes 8 (2020) 603.

[41] W. Leitner, J. Klankermayer, S. Pischinger, H. Pitsch, K. Kohse-Hoinghaus, Advanced biofuels and beyond: chemistry solutions for propulsion and production, Angew. Chem. Int. Ed. 56 (2017) 5412–5452.

[42] S.P. Elangovan, V. Krishnasamy, V. Murugesan, Synthesis, characterization and catalytic activity of ZAPO-5 and ZAPO-11, Catal. Lett. 36 (1996) 271–277.

[43] M. Tiemann, M. Schulz, C. Jager, M. Froba, Mesoporous aluminophosphate molecular sieves synthesized under nonaqueous condition, Chem. Mater. 13 (2001) 2885–2891.

[44] J. El Haskouri, C. Guillem, J. Latorre, A. Beltrán, D. Beltrán, P. Amorós, The first pure mesoporous aluminium phosphonates and diphosphonates – new hybrid porous materials, Eur. J. Inorg. Chem. 2004 (2004) 1804–1807.

[45] E. Welter, R. Chernikov, M. Herrmann, R. Nemausat, A Beamline for Bulk Sample X-ray Absorption Spectroscopy at the High Brilliance Storage Ring PETRA III, AIP Conf. Proc. 2054 (2019) 040002.

[46] B. Ravel, M. Newville, ATHENA, ARTEMIS, HEPHAESTUS: data analysis for X-ray absorption spectroscopy using IFEFFIT, J. Synchrotron Radiat. 12 (2005) 537–541.

[47] S.K. Saha, S.B. Waghmode, Y. Kubota, Y. Sugi, Synthesis of AFI aluminophosphate molecular sieves partly substituted with magnesium by dry-gel conversion method, Mater. Lett. 58 (2004) 2918–2923.

[48] W. Fang, A. Riisager, Efficient valorization of biomass-derived furfural to fuel bio-additive over aluminum phosphate, Appl. Catal. B: Environ. 298 (2021) 120575.

[49] S.H. Jhung, Y.K. Hwang, J.-S. Chang, S.-E. Park, Effect of acidity and anions on synthesis of AFI molecular sieves in wide pH range of 3–10, Microporous Mesoporous Mater. 67 (2004) 151–157.

[50] B. Zibrowius, E. Löffler, M. Hunger, Multinuclear MAS n.m.r, and i.r. spectroscopic study of silicon incorporation into SAPO-5, SAPO-31, and SAPO-34 molecular sieves, Zeolites 12 (1992) 167–174.

[51] R. Lookman, P. Grobet, R. Merckx, K. Vlassak, Phosphate sorption by synthetic amorphous aluminium hydroxides: a ^{27}Al and ^{31}P solid-state MAS NMR spectroscopy study, Eur. J. Soil Sci. 45 (1994) 37–44.

[52] N.N. Tušar, V. Kaučič, S. Geremia, G. Vlaic, A zinc-rich CHA-type aluminophosphate, Zeolites 15 (1995) 708–713.

[53] Y. Seo, S. Lee, C. Jo, R. Ryoo, Microporous aluminophosphate nanosheets and their nanomorphic zeolite analogues tailored by hierarchical structure-directing amines, J. Am. Chem. Soc. 135 (2013) 8806–8809.

[54] M. Othmani, A. Aissa, C.G. Bac, F. Rachdi, M. Debbabi, Surface modification of calcium hydroxyapatite by grafting of etidronic acid, Appl. Surf. Sci. 274 (2013) 151–157.

[55] N. Noroozi Pesyan, A. Gharib, M. Behroozi, A. Shokr, New full-substituted cyclopropanes derived from the one-pot reaction of meldrum's acid with aldehydes and BrCN in the presence of Et_3N, Arab. J. Chem. 10 (2017) S1558–S1566.

[56] K.L. Luska, A. Bordet, S. Tricard, I. Sinev, W. Grünert, B. Chaudret, W. Leitner, Enhancing the catalytic properties of ruthenium nanoparticle-SILP catalysts by dilution with iron, ACS Catal. 6 (2016) 3719–3726.

[57] P. Zhao, B. Boekfa, T. Nishitoba, N. Tsunoji, T. Sano, T. Yokoi, M. Ogura, M. Ehara, Theoretical study on ^{31}P NMR chemical shifts of phosphorus-modified CHA zeolites, Microporous Mesoporous Mater 294 (2020) 109908.

[58] C. Coelho, T. Azaïs, L. Bonhomme-Coury, G. Laurent, C. Bonhomme, Efficiency of the refocused $^{31}P-^{29}Si$ MAS-J-INEPT NMR experiment for the characterization of silicophosphate crystalline phases and amorphous gels, Inorg. Chem. 46 (2007) 1379–1387.

[59] W. Cai, R.D. Piner, F.J. Stadermann, S. Park, M.A. Shaibat, Y. Ishii, D. Yang, A. Velamakanni, S.J. An, M. Stoller, J. An, D. Chen, R.S. Ruoff, Synthesis and solid-state NMR structural characterization of ^{13}C-labeled graphite oxide, Science 321 (2008) 1815–1817.

[60] K. Petrak, I. Degen, P. Beynon, Some 1-substituted quaternary imidazolium compounds and related polymers: qualitative and quantitative infrared analysis, J. Polym. Sci., Polym. Chem. Ed. 20 (1982) 783–793.

[61] D.A. Carter, J.E. Pemberton, Raman spectroscopy and vibrational assignments of 1- and 2-methylimidazole, J. Raman Spectrosc. 28 (1997) 939–946.

[62] T. Gutel, C.C. Santini, K. Philippot, A. Padua, K. Pelzer, B. Chaudret, Y. Chauvin, J.-M. Basset, Organized 3D-alkyl imidazolium ionic liquids could be used to control the size of in situ generated ruthenium nanoparticles? J. Mater. Chem. 19 (2009) 3624–3631.

[63] X. Li, G. Fan, C. Zeng, Synthesis of ruthenium nanoparticles deposited on graphene-like transition metal carbide as an effective catalyst for the hydrolysis of sodium borohydride, Int. J. Hydrog. Energy 39 (2014) 14927–14934.

[64] K. Hadjiivanov, J.-C. Lavalley, J. Lamotte, F. Maugé, J. Saint-Just, M. Che, FTIR study of CO interaction with Ru/TiO_2 catalysts, J. Catal. 176 (1998) 415–425.

[65] O. Dulaurent, M. Nawdali, A. Bourane, D. Bianchi, Heat of adsorption of carbon monoxide on a Ru/Al_2O_3 catalyst using a dsorption equilibrium conditions at high temperatures, Appl. Catal. A: Gen. 201 (2000) 271–279.

[66] C. Schuschke, C. Hohner, C. Stumm, M. Kettner, L. Fromm, A. Görling, J. Libuda, Dynamic CO adsorption and desorption through the ionic liquid layer of a Pt model solid catalyst with ionic liquid layers, J. Phys. Chem. C 123 (2019) 31057–31072.

[67] R.G. Greenler, R.K. Brandt, The origins of multiple bands in the infrared spectra of carbon monoxide adsorbed on metal surfaces, Colloids Surf. A Physicochem. Eng. Asp. 105 (1995) 19–26.

[68] S. Wegner, C. Janiak, Metal nanoparticles in ionic liquids, Top. Curr. Chem. 375 (2017) 65.

[69] M. Chen, N. Maeda, A. Baiker, J. Huang, Molecular insight into Pt-catalyzed chemoselective hydrogenation of an aromatic ketone by in situ modulation–excitation IR spectroscopy, ACS Catal. 2 (2012) 2007–2013.

[70] R. Paul, C. Sarkar, Y. Yan, Q.T. Trinh, B.S. Rao, C.W. Pao, J.F. Lee, W. Liu, J. Mondal, Porous-organic-polymer-triggered advancement of sustainable magnetic efficient catalyst for chemoselective hydrogenation of cinnamaldehyde, ChemCatChem 12 (2020) 3687–3704.

[71] W. Fang, S. Liu, A.K. Steffensen, L. Schill, G. Kastlunger, A. Riisager, On the role of Cu^+ and CuNi alloy phases in mesoporous CuNi catalyst for furfural hydrogenation, ACS Catal. 13 (2023) 8437–8444.

[72] X. Meng, Y. Yang, L. Chen, M. Xu, X. Zhang, M. Wei, A control over hydrogenation selectivity of furfural *via* tuning exposed facet of Ni catalysts, ACS Catal. 9 (2019) 4226–4235.

[73] C. Janiak, Ionic liquids for the synthesis and stabilization of metal nanoparticles, Z. Naturforsch. B 68 (2013) 1059–1089.

[74] K.L. Luska, P. Migowski, W. Leitner, Ionic liquid-stabilized nanoparticles as catalysts for the conversion of biomass, Green Chem. 17 (2015) 3195–3206.

[75] D. Krishnan, L. Schill, M.R. Axet, K. Philippot, A. Riisager, Ruthenium nanoparticles stabilized with methoxy-functionalized ionic liquids: synthesis and structure-performance relations in styrene hydrogenation, Nanomaterials 13 (2023) 1459.

[76] C. Muthuselvi, S.S. Pandiaraja, B. Ravikumar, S. Athimoolam, N. Srinivasan, R. V. Krishnakum, FT-IR and FT-Raman spectroscopic analyzes of indeno quinoxaline derivative crystal, Asian J. Appl. Sci. 11 (2018) 83–91.